Thermoelectric Transport in a Correlated Electron System on the Surface of Liquid Helium

Thermoelectric Transport in a Correlated Electron System on the Surface of Liquid Helium

Ivan Kostylev,* A. A. Zadorozhko, M. Hatifi, and Denis Konstantinov†
Quantum Dynamics Unit, Okinawa Institute of Science and Technology, Tancha 1919-1, Okinawa 904-0495, Japan

(Received 4 June 2021; accepted 21 September 2021; published 26 October 2021)

We report on the direct observation of the thermoelectric transport in a nondegenerate electron system trapped on the surface of liquid helium. The microwave-induced excitation of the vertical transitions of electrons between the surface-bound states results in their lateral flow, which we were able to detect by employing a segmented electrode configuration. We show that this flow of electrons arises due to the Seebeck effect. Our experimental results are in good agreement with the theoretical calculations based on kinetic equations. This demonstrates the importance of the fast electron-electron collisions, which, in particular, leads to the violation of the Wiedemann-Franz law in this system.

DOI: 10.1103/PhysRevLett.127.186801

Recently, there has been a renewed interest in the thermoelectric transport properties of materials [1]. Thermoelectric power generation, that is, conversion of the thermal energy into electric power under a temperature gradient through the Seebeck effect, is believed to be one of the key technologies for sustainable energy. Driven by desire to improve efficiency of the energy-conversion process, the interest has turned to systems other than conventional bulk solid-state semiconductors, such as low-dimensional mesoscopic structures [2–5], graphene sheets, and nanostructures [6], as well as organic-based materials [7]. The thermoelectric performance is a trade-off between different transport parameters, which intrinsically are determined by carrier scattering mechanisms in the system. Besides a large value of the Seebeck coefficient S, which relates the temperature gradient and the generated electromotive force, it is desired to have a large value of the electrical conductivity σ and a low value of the thermal conductivity κ. This is summarized in the dimensionless figure of merit ZT at a given temperature T as $ZT = (S^2\sigma/\kappa)T$. The thermoelectric performance of modern solid-state systems is still rather poor [8–10], with a maximum value of $ZT = 2.6$ [11]. The challenge for increasing ZT arises from the coupling between the transport coefficients S, σ, and κ and decoupling these parameters is nontrivial. It is believed that study of the thermoelectric transport in controllable model systems, such as cold atoms [12–14] and ions [15,16], is important for fundamental understanding of the problem.

Electrons trapped on the surface of liquid helium present an extremely clean and controllable nondegenerate Coulomb system [17]. The bound states of such surface electrons (SEs) are formed due to an attractive image-charge potential and a repulsive barrier at the surface. Trapped electrons are free to move laterally along the surface and scatter only from helium vapor atoms, whose density is negligible at temperatures sufficiently below 1 K, or the surface capillary waves (ripplons). Thus, the system is free of static disorder typical for solid-state systems. Electric transport measurements reveal the highest electron mobility known in any charge systems [18]. Much less is known about the thermal and thermoelectric transport of SEs on helium. Recently, it was demonstrated that the Seebeck effect can be used to probe the temperature of SEs in the vapor-atom scattering regime at 1.6 K [19]. In this Letter, the electron-electron interaction was omitted from the discussion. However, theoretically it is expected that very fast inelastic electron-electron scattering, which is a signature of strongly correlated electron liquid on liquid helium [20], can lead to violation of the Wiedemann-Franz law and significant increase of the ratio σ/κ [21–23]. Thus, a careful study of thermoelectric transport in this controllable disorder-free system can potentially help us to explore different regimes of thermoelectric transport for energy-conversion optimization.

In this Letter, we report direct observation of the thermoelectric transport of electrons on the surface of liquid helium. We used resonant microwave excitation of the electron transitions between surface-bound states to heat SEs locally with a high spatial resolution, while, by employing a segmented geometry of the electrodes coupled to SEs, we were able to extract a signal corresponding to charge flow along the surface. We find that the net particle current is always directed from the hot place to the cold place, which is the signature of the Seebeck effect. The magnitude of the thermoelectric current, its nonlinear microwave-power dependence, as well as its dynamic response, are all in a good agreement with our calculations based on the kinetic equations. Interestingly, by taking into account extremely fast inelastic electron-electron

collisions, the theoretically estimated figure of merit ZT can reach values much larger than unity due to violation of the Wiedemann-Franz law.

In our experiment SEs, of typical number density $n_s \approx 10^7$ cm^{-2}, are trapped on a free surface of liquid ^{3}He placed between two circular electrodes and cooled below 1 K inside a leak-tight experimental cell attached to the cold plate of a refrigerator. The electrodes, each of 24 mm diameter, form a parallel-plate capacitor with a gap $d = 2.1$ mm between the top and bottom plates, and the liquid level is placed approximately midway between the plates. Electrons form a round pool of surface charge when a positive voltage is applied to the bottom plate. SEs can be exposed to a microwave (MW) radiation at the frequency ~100 GHz transmitted from a room temperature source into the cell via a waveguide. The frequency of transitions between the surface-bound states of SEs can be tuned in resonance with the applied radiation via the Stark shift by varying the electric field $E_\perp$ in the capacitor gap. As was recently demonstrated, the vertical displacement of electrons due to their excitation to higher surface states can be detected by measuring the change in the image charge induced by SEs at the capacitor plates [24]. A pulse-modulated MW excitation causes a modulated image current in the plates whose first harmonic can be measured by a conventional lock-in amplifier. The image-charge currents induced in the top and bottom plates have the same magnitude and opposite polarities. In the experiment described here, a simple but important modification of this experimental setup was introduced. Particularly, each round plate of the capacitor was segmented into three concentric electrodes by two circular gaps of diameters 13 and 18 mm, each having a width of about 0.2 mm, as shown schematically in Fig. 1(a). By applying separate electrical potentials to different segments, the size of the electron pool, as well as the value of the tuning electric field $E_\perp$ at different parts of the system, can be varied. As an example, the calculated SE density profile when a positive potential is applied to the central and middle segments of the bottom electrode ($V_{bc} = V_{bm} = +17.8$ V), while all other segments are grounded, is shown in Fig. 1(a). Additionally, the image currents due to displacement of SEs can be measured at each segment independently. As shown below, such a setup allowed us to reveal a strong lateral motion of SEs due to pulse-modulated resonant MW excitation, in addition to the vertical displacement of SEs due to occupation of the higher surface states.

Figure 1(b) shows the image currents I_{tc} (solid black line) and I_{bc} (dashed black line) at the central segments of the top and bottom plates, respectively, for SEs under pulse-modulated MW excitation at frequency $\omega/2\pi = 130$ GHz for different values of a positive voltage V_b ($= V_{bc} = V_{bm}$) applied simultaneously to the central and middle segments of the bottom plate. A nonzero current response around $V_b = 17.8$ V, which corresponds to the electric field

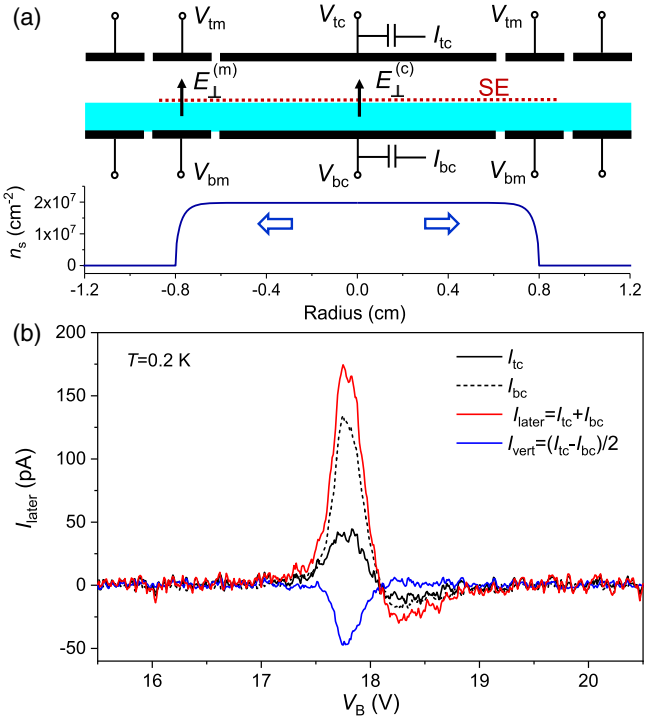

FIG. 1. (a) Schematic view of the segmented electrode geometry used in the experiment and the equilibrium electron density profile calculated as described in the text. The horizontal arrows indicate direction of electron flow induced by resonant MW excitation. (b) The image-current response obtained at $T = 200$ mK using pulse-modulated ($f_m = 400$ kHz) excitation of SEs by 130-GHz radiation. The measured image currents I_{tc} and I_{bc} at the central segments of the capacitor's top and bottom plates, respectively, are plotted by solid (black) and dashed (black) lines, respectively.

$E_\perp = V/d \approx 85$ V/cm, indicates the MW-induced excitation of SEs from the ground state to the first excited state. Contrary to what is expected from the vertical displacement of electrons, the magnitude of measured currents I_{tc} and I_{bc} differs significantly. It is clear that at resonance, in addition to the vertical displacement of SEs seen earlier [24], there is also a strong in-plane displacement of SEs. Thanks to our geometry, it is straightforward to eliminate the contribution to measured currents from the vertical displacement of SEs by adding the two measured currents together. The sum of two image currents, $I_{later} = I_{bc} + I_{tc}$, is shown by a solid red line in Fig. 1. This signal corresponds to the depletion of the negative surface charge due to SEs located between the central segments and therefore the lateral displacement of SEs away from the center of the electron pool. We have confirmed that the sum of two currents measured at the middle segments of bottom and top plates, respectively, is nearly equal in magnitude and opposite in sign to I_{later}, as should be expected from the charge conservation. Also, since the lateral displacement of SEs must induce equal changes in the image charges at the top and bottom segments, providing the liquid level is at the middle

between the capacitor plates, the signal due to the vertical displacement of SEs induced, for example, at the top plate can be recovered by subtracting the measured currents, that is $I_{\rm vert} = (I_{\rm tc} - I_{\rm bc})/2$. This quantity is shown by the solid blue line in Fig. 1(b). As expected, this signal is similar to the one measured earlier [24].

Using this procedure, we can investigate, in detail, dependence of the electron lateral displacement on various experimental parameters. Of particular interest is the displacement direction within the electron pool. For the data shown in Fig. 1(a), SEs occupying areas between the central and middle segments are tuned in resonance simultaneously and $I_{\rm later}$ is positive. The segmented geometry of electrodes allows us to tune these two parts of the electron pool independently while retaining the same electrical potentials at the surface to keep the same equilibrium electron density profile. To accomplish this, we apply the following voltages: $V_{\rm bc} = V_1$, $V_{\rm tc} = 0$, $V_{\rm bm} = V_1 + V_2$, and $V_{\rm tm} = -V_2$, where V_1 and V_2 can be varied independently. It is clear that this configuration of potentials satisfies the above requirements. Particularly, the tuning electric fields for SEs between the central and middle segments are given by $E_\perp^{(c)} = V_1/d$ and $E_\perp^{(m)} = (V_1 + 2V_2)/d$, respectively, as shown schematically in Fig. 1(a). Figure 2 shows a color map of $I_{\rm later}$ versus $E_\perp^{(c)}$ and $E_\perp^{(m)}$ obtained for SEs under pulse-modulated MW excitation as described above. Particular care was taken to ensure a uniform density profile for SEs above the middle electrode. The lateral displacement current is positive (red color) when SEs at the central part of the electron pool are tuned in resonance with the applied radiation. Contrarily, the current is negative (blue color) when SEs in the peripheral part of the electron pool are tuned to the resonance. This corresponds to the lateral displacement of SEs from the peripheral part of the electron pool toward the center. The data in Fig. 2 unequivocally confirm that under irradiation SEs are displaced from the part of the pool where they are resonantly excited toward the part where they are off resonance. In particular, this explains the change in the sign of $I_{\rm later}$ on the high-voltage side of the resonance peak in Fig. 1(b). Indeed, at such fields SEs at the edge of the electron pool, which experience somewhat lower $E_\perp$ field than the rest of the SEs, become tuned to the resonance, while the rest of the pool is already detuned. Correspondingly, electrons displace from the resonantly excited edge of the pool toward its center, which results in $I_{\rm later} < 0$.

It is well established that MW-induced excitation of the surface states of SEs on liquid helium heats the electron system due to decay of the excited SEs caused by elastic collisions with vapor atoms and ripplons [25,26]. Such collisions, in a typical timescale $10^{-8} - 10^{-10}$ s in the temperature range 0.2–0.6 K considered here, provide an effective channel to transfer excitation energy absorbed by SEs from the MW field to the electron thermal energy [26].

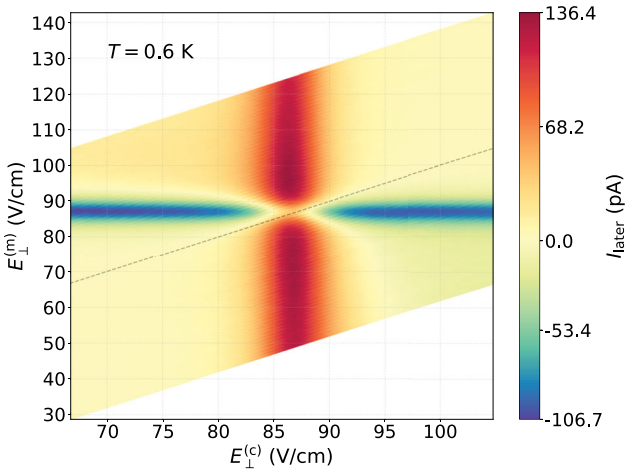

FIG. 2. Color map of the measured lateral displacement current $I_{\rm later}$ versus $E_\perp^{(c)}$ and $E_\perp^{(m)}$ for SEs under pulse-modulated ($f_m = 200$ kHz) excitation by 130-GHz radiation at $T = 600$ mK. The dashed line marks $E_\perp^{(c)} = E_\perp^{(m)}$.

The thermal equilibrium among the irradiated electrons, with an effective electron temperature $T_e > T$, is established on a timescale of the inelastic electron-electron collisions, which is on the order 10^{-10} s for electron densities considered here [20]. The electron temperature is determined by balance between the energy gain due to MW absorption and energy loss due to inelastic collisions of SEs with scatterers. The latter is slow, in a timescale $10^{-6} - 10^{-7}$ s for typical temperatures considered here [27]. This allows overheating of the MW-excited SEs to a few degrees Kelvin above the bath temperature T for typical MW powers used in the experiment. Finally, the heat can propagate in the electron system through the electronic thermal conductance.

The thermoelectric transport in SEs must be described by kinetic equations taking into account elastic scattering of electrons from vapor atoms and ripplons, as well as inelastic electron-electron collisions. According to Ref. [23] (see also an earlier work by Keyes [28]), the Boltzmann equation in the relaxation-time approximation (RTA) for a many-electron system can be presented as

$$\frac{\partial f}{\partial t} + \mathbf{v}\nabla f + \dot{\mathbf{p}}\nabla_{\mathbf{p}} = -\frac{f - f_0}{\tau} - \frac{f - f_0^*}{\tau_{ee}}, \qquad (1)$$

where $f = e^{(\mu-\epsilon)/\beta}$ is the distribution function for nondegenerate electrons [μ is the chemical potential, ε is the electron total energy, and $\beta = (k_B T_e)^{-1}$], f_0 and f_0^* is the equilibrium distribution in the laboratory and center-of-mass frames, respectively, τ is the electron momentum relaxation time due to elastic scattering from vapor atoms and ripplons, and τ_{ee} is the electron-electron scattering time. Following Ref. [23], it is straightforward to obtain the thermoelectric transport coefficients S, σ, and κ. For the

stationary state of the electron system, where no electric current flows, we obtain [29]

$$\sigma = \frac{e^2 n_s \tau}{m_e}, \qquad S = -\frac{k_B}{e}(2 - \mu\beta + \langle E_n \rangle \beta),$$
$$\kappa = \frac{n_s \tilde{\tau}}{m_e T_e}(2\beta^{-2} + \langle E_n^2 \rangle - \langle E_n \rangle^2). \tag{2}$$

Here, $\tilde{\tau} = (\tau^{-1} + \tau_{ee}^{-1})^{-1}$, E_n is the quantized energy of electron vertical motion, and $\langle .. \rangle$ denotes the thermal average. Note that, for the sake of simplicity, we consider momentum-independent scattering time τ, which is valid for elastic scattering by vapor atoms dominating at $T > 0.3$ K for SEs on liquid ^{3}He. Using the above expressions and azimuthal symmetry of our experimental setup, we can find the current response of the electron system to resonant heating by solving the coupled partial differential equations for electron temperature $T_e(r,t)$ and electron density $n_s(r,t)$

$$\frac{\partial T_e}{\partial t} = W_{\text{abs}} - W_{\text{loss}} + \frac{1}{n_s r}\frac{\partial}{\partial r}\left(\kappa r \frac{\partial T_e}{\partial r}\right),$$
$$\frac{\partial n_s}{\partial t} = \frac{\sigma}{Cr}\frac{\partial}{\partial r}\left(r\frac{\partial n_s}{\partial r}\right) - \frac{\sigma S}{er}\frac{\partial}{\partial r}\left(r\frac{\partial T_e}{\partial r}\right). \tag{3}$$

The first expression is the heat conduction equation, where W_{abs} and W_{loss} (divided by k_B) is the rate of energy absorption and energy loss per electron, respectively. The former depends on the value of MW electric field E_{MW} inside the cell, while the latter is determined by the inelastic scattering of electrons. The second expression is the continuity equation, where we used relation for the electric current density $j_e = -\sigma\nabla\phi - \sigma S \nabla T_e$ (see Supplemental Material [29]). The electric potential of SEs ϕ is related to their density by the Poisson equation. Here, for the sake of simplicity, we used a capacitance model for small variations of ϕ and n_s around their equilibrium values, $\delta\phi = -e\delta n_s/C$, where $C = 2\epsilon_0/d \approx 1.8 \times 10^{-8}$ F/m^2 [29].

In order to make comparison with our calculations, we performed real-time measurements of $I_{\text{later}}(t)$ for SEs tuned in resonance with the pulse-modulated MW radiation using a fast current preamplifier (FEMTO® DHPCA-100). The transient current traces for different values of the output power P_{MW} of our MW source are shown in Fig. 3(a). For the sake of comparison, a representative trace calculated using Eqs. (3) for $E_{\text{MW}} = 0.42$ V/m, with a 2 MHz low-pass filter applied to match the experimental conditions [29], is also shown by the dashed black line. Figure 3(b) shows the power dependence of I_{later} measured directly by the lock-in amplifier (open red circles), as well as the first harmonic extracted from the measured transient current traces (closed blue circles). As expected, we get essentially identical results. For the sake of comparison, the first harmonic extracted from the calculated traces for different values of $E_{\text{MW}}^2 \propto P_{\text{MW}}$ is plotted by the dashed line. Note that an exact relation between the output power P_{MW} and the electric field E_{MW} cannot be accurately determined. For this reason, the range of E_{MW} (the top axis) is adjusted to give the best match between the theory and experiment. The observed nonlinearity of the power dependence, which stems from the nonlinear power dependence of T_e, is reproduced well by our calculations. We note that this peculiar nonlinearity allows us to rule out some other explanations of the observed lateral current, for example, due to a photogalvanic effect, which would produce a linear power dependence [33].

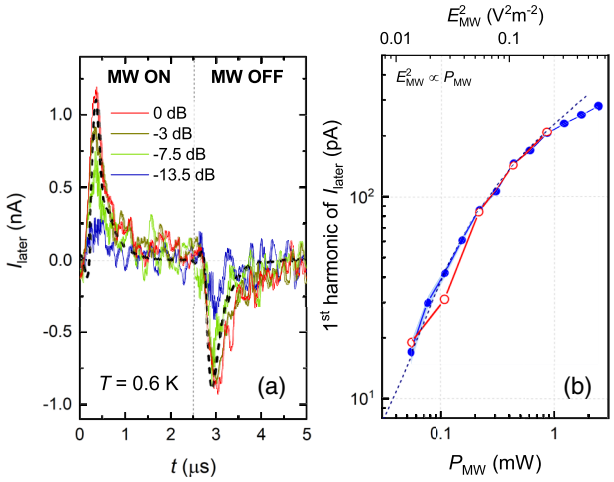

FIG. 3. (a) Measured transient traces of $I_{\text{later}}(t)$ for SEs under pulsed-modulated ($f_{\text{m}} = 200$ kHz) 130-GHz radiation for different values of the MW-source power (indicated in decibels with respect to the maximum power). The dashed black line is the current response calculated using Eqs. (3) for $E_{\text{MW}} = 0.42$ V/m. (b) The first harmonic of $I_{\text{later}}(t)$ measured by the lock-in amplifier (open red circles) and extracted from transient traces shown in (a) (closed blue circles) versus input MW power P_{MW}. Dashed line represents I_{later} versus E_{MW}^2 extracted from the calculated transient traces (see Supplemental Material [29]).

In summary, we reported direct observation of the thermoelectric transport in a 2D electron liquid due to a nonuniform heating of the system by resonant MW radiation. Our results are in good agreement with the calculations based on kinetic equations. This Letter provides the opportunity to study thermoelectricity in a clean system with controllable parameters, which can affect electric and thermal properties of the system in a nontrivial way. In particular, the figure of merit ZT obtained from Eqs. (3) can significantly exceed unity. By using the estimates $S \approx -2(k_B/e)$ and $\kappa \approx (2k_B T_e n_s \tilde{\tau})/m_e$, we obtain $ZT \approx 2(\tau/\tilde{\tau})$. This varies between 4 and 350 for the temperature range between 0.6 and 0.2 K due to the fact that $\tau_{ee} \ll \tau$ in the electron-on-helium system. Such enormous values of ZT are possible due to decoupling between the transport coefficients σ and κ: while the electron-electron collisions cannot affect the momentum relaxation

due to the conservation of momentum, they strongly affect relaxation of the thermal current. This is equivalent to violation of the Wiedemann-Franz law [21–23]. However, we note that the above theoretical results are obtained under an assumption of RTA with a phenomenological parameter τ_{ee}. Further studies are required to check validity of these estimates. In particular, an experiment is required to measure the thermoelectric transport coefficients directly. This can be accomplished by employing a two-terminal setup with local measurements of the electron temperature, in the spirit of recent works done with cold atoms [12–14]. In SEs on liquid helium, such a setup can be realized in a microchannel structure filled with superfluid helium, which typically consists of two reservoirs connected by a narrow channel [34]. This can open different possibilities to use SEs on liquid helium as an experimental platform for many-body quantum simulators of thermoelectricity and nano-friction [35,36].

This work was supported by an internal grant from Okinawa Institute of Science and Technology (OIST) Graduate University.

*ivan.kostylev@oist.jp
†denis@oist.jp

[1] G. J. Snyder and E. S. Toberer, Nat. Mater. **7**, 105 (2008).
[2] V. Narayan, M. Pepper, and D. A. Ritchie, C. R. Phys. **17**, 1123 (2016).
[3] A. I. Hochbaum, R. Chen, R. D. Delgado, W. Liang, E. C. Garnett, M. Najarian, A. Majumdar, and P. Yang, Nature (London) **451**, 163 (2008).
[4] A. I. Boukai, Y. Bunimovich, J. Tahir-Kheli, J.-K. Yu, W. A. Goddard III, and J. R. Heath, Nature (London) **451**, 168 (2008).
[5] S. Shimizu, M. S. Bahramy, T. Iizuka, S. Ono, K. Miwa, Y. Tokura, and Y. Iwasa, Proc. Natl. Acad. Sci. U.S.A. **113**, 6438 (2016).
[6] P. Zong, J. Liang, P. Zhang, C. Wan, Y. Wang, and K. Koumoto, ACS Appl. Energy Mater. **3**, 2224 (2020).
[7] B. Russ, A. Glaudell, J. J. Urban, M. L. Chabinyc, and R. A. Segalman, Nat. Rev. Mater. **1**, 16050 (2016).
[8] R. Venkatasubramanian, E. Siivola, T. Colpitts, and B. O'Quinn, Nature (London) **413**, 597 (2001).
[9] B. Poudel, Q. Hao, Y. Ma, Y. Lan, A. Minnich, B. Yu, X. Yan, D. Wang, A. Muto, D. Vashaee, X. Chen, J. Liu, M. S. Dresselhaus, G. Chen, and Z. Ren, Science **320**, 634 (2008).
[10] K. Biswas, J. He, I. D. Blum, C.-I Wu, T. P. Hogan, D. N. Seidman, V. P. Dravid, and M. G. Kanatzidis, Nature (London) **489**, 414 (2012).
[11] L.-D. Zhao, S.-H. Lo, Y. Zhang, H. Sun, G. Tan, C. Uher, C. Wolverton, V. P. Dravid, and M. G. Kanatzidis, Nature (London) **508**, 373 (2014).
[12] J.-P. Brantut, C. Grenier, J. Meineke, D. Stadler, S. Krinner, C. Kollath, T. Esslinger, and A. Georges, Science **342**, 713 (2013).
[13] C. Grenier, C. Kollath, and A. Georges, C. R. Phys. **17**, 1161 (2016).
[14] S. Krinner, T. Esslinger, and J.-P. Brantut, J. Phys. Condens. Matter **29**, 343003 (2017).
[15] O. V. Zhirov and D. L. Shepelyansky, Europhys. Lett. **103**, 68008 (2013).
[16] O. V. Zhirov, J. Lages, and D. L. Shepelyansky, Eur. Phys. J. D **73**, 149 (2019).
[17] Yu. P. Monarkha and Kono, *Two-Dimensional Coulomb Liquids and Solids* (Springer-Verlag, Berlin, 2004).
[18] *Two-Dimensional Electron Systems on Helium and Other Cryogenic Substrates*, edited by E. Y. Andrei (Kluwer Academics, Dordrecht, MA, 1997).
[19] E. I. Kleinbaum and S. A. Lyon, Phys. Rev. Lett. **121**, 236801 (2018).
[20] C. L. Zipfel, T. R. Brown, and C. C. Grimes, Phys. Rev. Lett. **37**, 1760 (1976).
[21] A. Principi and G. Vignale, Phys. Rev. Lett. **115**, 056603 (2015).
[22] A. Lucas and S. Das Sarma, Phys. Rev. B **97**, 245128 (2018).
[23] W.-R. Lee, A. M. Finkel'stein, K. Michaeli, and G. Schwiete, Phys. Rev. Research **2**, 013148 (2020).
[24] E. Kawakami, A. Elarabi, and D. Konstantinov, Phys. Rev. Lett. **123**, 086801 (2019).
[25] A. P. Volodin and V. S. Édel'man, Sov. Phys. JETP **54**, 198 (1981), http://www.jetp.ras.ru/cgi-bin/e/index/e/54/1/p198?a=list.
[26] D. Konstantinov, H. Isshiki, Yu. P. Monarkha, H. Akimoto, K. Shirahama, and K. Kono, Phys. Rev. Lett. **98**, 235302 (2007).
[27] E. Kawakami, A. Elarabi, and D. Konstantinov, Phys. Rev. Lett. **126**, 106802 (2021).
[28] R. W. Keyes, J. Phys. Chem. Solids **6**, 1 (1958).
[29] See Supplemental Material at http://link.aps.org/supplemental/10.1103/PhysRevLett.127.186801 for derivation of thermoelectric transport coefficients and numerical solution of time-dependent heat conduction and continuity equations, which includes Refs. [30–32].
[30] D. Konstantinov, H. Isshiki, H. Akimoto, K. Shirahama, Yu. Monarkha, and K. Kono, J. Phys. Soc. Jpn. **77**, 034705 (2008).
[31] T. Ando, J. Phys. Soc. Jpn. **44**, 765 (1978).
[32] L. Wilen and R. Giannetta, J. Low Temp. Phys. **72**, 353 (1988).
[33] M. V. Entin and L. I. Magarill, JETP Lett. **98**, 816 (2014).
[34] J.-Y. Lin, A. V. Smorodin, A. O. Badrutdinov, and D. Konstantinov, J. Low Temp. Phys. **195**, 289 (2019).
[35] D. Mandelli and E. Tosatti, Nature (London) **526**, 332 (2015).
[36] E. Altman *et al.*, PRX Quantum **2**, 017003 (2021).